Xie et al. Cell Division (2024) 19:27
https://doi.org/10.1186/s13008-024-00131-z

Cell Division

RESEARCH Open Access

Overexpression of ZFP69B promotes hepatocellular carcinoma growth by upregulating the expression of TLX1 and TRAPPC9

Wei Xie[1†], Zhongming Bao[2†], Dan Yao[3] and Yong Yang[4*]

Abstract

Background T-cell leukemia homeobox protein 1 (TLX1) has been revealed as a hub transcription factor in leukemia, while its function in hepatocellular carcinoma (HCC) has not been well described. Here, we investigated the regulation and function of TLX1 in HCC.

Methods TLX1 and its possible upstream and downstream molecules in HCC were identified using bioinformatics tools, which were then verified by RT-qPCR assay. CCK-8, wound healing, and Transwell invasion assays were performed to detect the effects of TLX1 knockdown on HCC cells. The interactions between TLX1 and trafficking protein particle complex subunit 9 (TRAPPC9) or Zinc finger protein 69 homolog B (ZFP69B) were further probed by ChIP and luciferase reporter assays. Rescue experiments were finally conducted in vitro and in vivo.

Results TLX1 was highly expressed in HCC cells, and the knockdown of TLX1 led to reduced malignant biological behavior of HCC cells. TLX1 bound to the promoter region of TRAPPC9, thereby promoting TRAPPC9 expression. Overexpression of TRAPPC9 attenuated the effect of TLX1 reduction on suppressing malignant behavior of HCC cells. ZFP69B was also highly expressed in HCC cells and bound to the promoter region of TLX1 to induce TLX1 expression. Knockdown of ZFP69B inhibited the viability and mobility of HCC cells in vitro and tumor growth in vivo, and overexpression of TLX1 rescued this inhibition.

Conclusion These findings suggest that ZFP69B promotes the proliferation of HCC cells by directly upregulating the expression of TLX1 and the ensuing TRAPPC9.

Keywords Hepatocellular carcinoma, ZFP69B, TLX1, TRAPPC9

†Wei Xie and Zhongming Bao contributed equally to this work.

*Correspondence:
Yong Yang
yangyongdoc@163.com
[1]Department of General Surgery, Jurong Hospital Affiliated to Jiangsu University, Zhenjiang, Jiangsu 212400, P.R. China
[2]Department of Hepatobiliary Surgery, Huai'an Fifth People's Hospital, Huaiyin, Jiangsu 223300, P.R. China
[3]Department of Gastrointestinal Surgery, Huai'an Second People's Hospital (Huai'an Hospital Affiliated to Xuzhou Medical University), Huai'an, Jiangsu 223001, P.R. China
[4]Department of Hepatobiliary and Pancreatic Surgery, the Affiliated Hospital of Xuzhou Medical University, No. 99, Huaihai West Road, Quanshan District, Xuzhou, Jiangsu 221000, P.R. China

Background

Liver cancer is the sixth most common malignant tumor and the third leading cause of cancer-related death in 2020 according to the GLOBOCAN database [1], and hepatocellular carcinoma (HCC) accounts for around 90% of primary malignant liver tumors [2, 3]. Due to delays in diagnosis at early asymptomatic stages, HCC develops into a severe aggressive stage, thereby having a significant negative impact on patient survival [4]. Recent advances in systemic and locoregional therapies have contributed to alteration in many guidelines regarding systemic treatment and the possibility of downstage patients undergoing resection [5].

Homeobox (Hox) genes are homeodomain transcription factors (TF) that are involved in the control of key processes in metazoan development [6]. In the context of cancer development, the abnormal expression of Hox genes may affect cell proliferation, apoptosis, motility, angiogenesis, and autophagy [7]. Among them, HOX11 (also known as T-cell leukemia homeobox protein 1, TLX1), belonging to the NKL family of homeobox transcription factors and regulating the transcription of many genes, has been implicated in the development of T-cell acute lymphoblastic leukemias [8]. Moreover, the migration abilities of bladder cancer cells were decreased after the knockdown of TLX1 [9]. However, the specific role of TLX1 has not been expounded in HCC. In the present study, we identified TLX1 as a hub TF in the progression of HCC by combining two GEO datasets and the HumanTFDB (http://bioinfo.life.hust.edu.cn/HumanTFDB#!/download). In addition, trafficking protein particle complex subunit 9 (TRAPPC9, also known as NIK- and IKKβ-binding protein, NIBP) and zinc finger protein 69 homolog B (ZFP69B, also termed ZNF643) were obtained as its downstream target and upstream modifier, respectively. TRAPPC9 is a protein subunit of the transport protein particle II and has been reported to be involved in breast and colon cancers and liver diseases [10]. In addition, the relative expression of TRAPPC9 in esophageal cancer tissues was higher than those in adjacent normal tissues, and TRAPPC9 levels in tumor tissues with lymph node metastasis were significantly higher than those in tissues without lymph node metastasis [11]. ZFP proteins have been reported in various diseases, especially in cancers, including HCC [12]. For instance, the downregulation of ZNF384 suppressed HCC cell proliferation by inhibiting the expression of Cyclin D1 [13]. More relevantly, ZFP69B has been revealed as one of the seven genes that are related to cuproptosis and ferroptosis in HCC [14]. Nevertheless, the detailed role of TRAPPC9 and ZFP69B played in HCC is not fully elucidated. Herein, we sought to explore the influence of ZFP69B on HCC development via the TLX1/TRAPPC9 axis. The objective was to provide a potential basis for HCC treatment.

Results

TLX1 is highly expressed in HCC tissues and cell lines

Two GEO datasets concerning HCC were included to analyze the transcriptome changes in HCC: GSE87410 (Fig. 1A) and GSE105130 (Fig. 1B). In addition, we downloaded the human TF and human TF cofactors on HumanTFDB and obtained the intersecting genes (Fig. 1C) with the above two datasets, with a total of 225 intersections.

We performed a KEGG pathway enrichment analysis of 225 intersecting genes on Hiplot (https://www.hiplot.com.cn/), and the results showed that these intersecting genes were mainly enriched in Transcriptional misregulation in cancer pathway (Fig. 1D). We then analyzed the 11 genes enriched in the Transcriptional misregulation in cancer and plotted a heatmap (Fig. 1E). All genes have been studied in liver cancer except PBX1, RXRB, and TLX1. Among the three genes, TLX1 was the most significantly differentially expressed in HCC, with Log_2FoldChange of 3.875825 (GSE87410) and 3.1132641 (GSE105130), respectively, so we chose TLX1 for further study.

We then examined the expression of TLX1 in 31 pairs of HCC and matched adjacent tissues by RT-qPCR and immunohistochemistry. TLX1 was significantly higher in tumor tissues than in adjacent tissues (Fig. 1F, G). Based on the mean value of TLX1 mRNA expression as a threshold, patients were classified into TLX1 high and low expression groups and the correlation between TLX1 and clinical characteristics of patients was shown in Table 1. TLX1 was not associated with the age and sex of patients. However, patients with high expression of TLX1 tended to have larger tumor sizes and more advanced TNM stages (Table 1). Besides, the expression of TLX1 in THLE-2 cells was also lower than that in Huh-7 and MHCC97H cells (Fig. 1H).

Knockdown of TLX1 inhibits biological behavior of Huh-7 and MHCC97H cells

To determine the effect of TLX1 on the biological behavior of HCC cells, we infected Huh-7 and MHCC97H cells with sh-TLX1 or sh-NC and verified the knockdown efficiency by RT-qPCR assay (Fig. 2A). The HCC cell proliferation rate reflected by CCK-8 was significantly reduced after TLX1 was knocked down (Fig. 2B). HCC cells infected with sh-TLX1 also healed significantly slower than the sh-NC group in the wound healing assay (Fig. 2C). Similarly, the number of invaded cells was less in the sh-TLX1 group than in the sh-NC group (Fig. 2D). In addition, we also knocked down TLX1 in HepG2 and SNU-398 cells, and RT-qPCR verified the knockdown

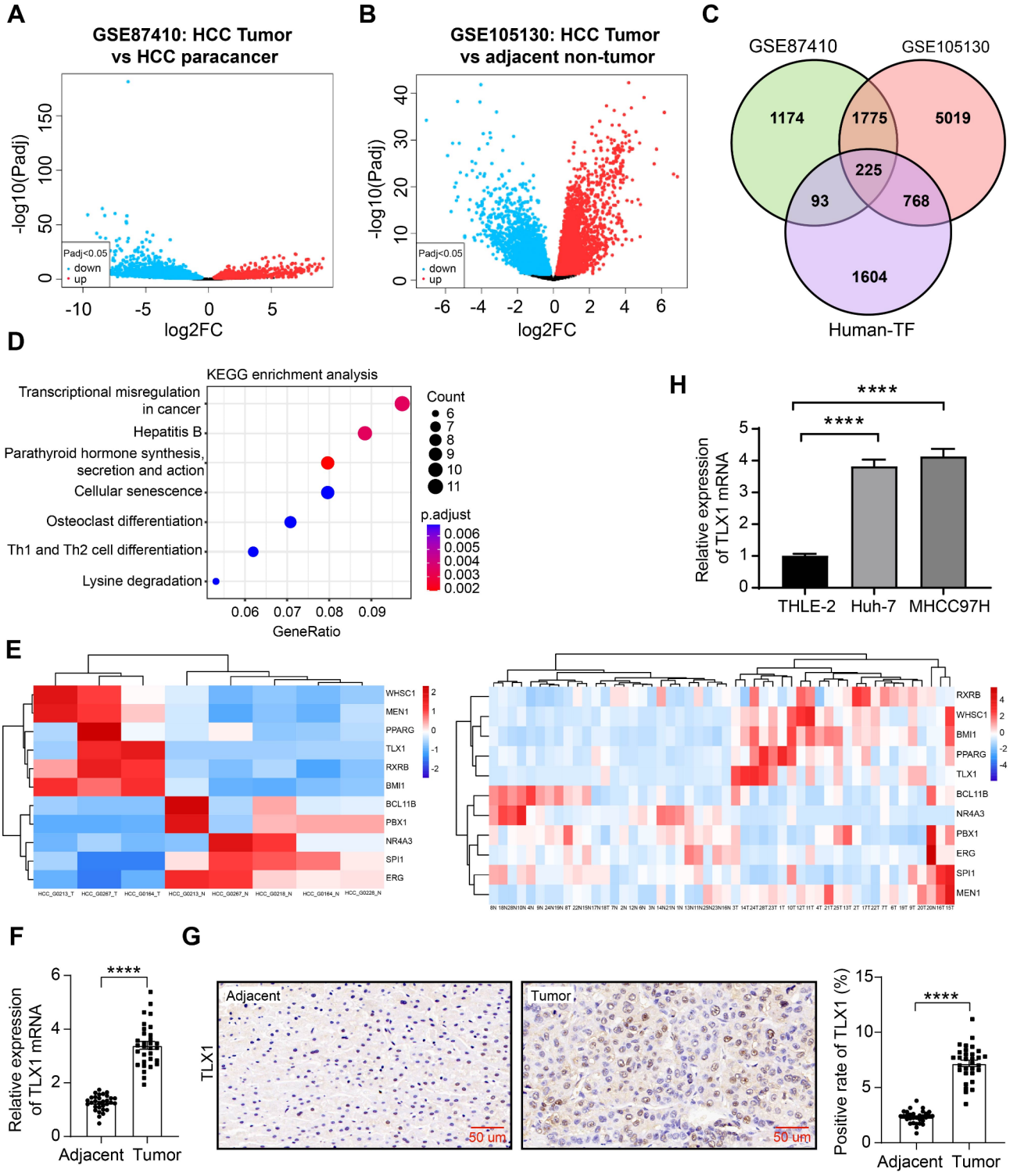

Fig. 1 Overexpression of TLX1 is identified in HCC tissues and cell lines. (**A**) Transcriptome differences between HCC and paracancerous tissues in the GSE87410 dataset. (**B**) Transcriptome differences between HCC and adjacent non-tumor in the GSE105130 dataset. (**C**) Intersection of the above two datasets with human transcription factors and transcription cofactors in Jvenn. (**D**) KEGG pathway enrichment analysis of 225 intersecting genes. (**E**) Heatmaps of 11 intersecting genes enriched in the Transcriptional misregulation in cancer pathway in the GSE87410 and GSE105130 datasets. (**F**) mRNA expression of TLX1 in HCC tissues and their adjacent tissues was analyzed using RT-qPCR ($n=31$). (**G**) positive staining of TLX1 in HCC tissues and their adjacent tissues was analyzed using immunohistochemistry ($n=31$). (**H**) TLX1 mRNA expression in THLE-2, Huh-7, and MHCC97H cells was analyzed using RT-qPCR. Data represent the mean ± SEM of at least three independent experiments. ****$p<0.0001$. Differences were tested using a paired t-test (F, G) and the one-way ANOVA (**H**)

Table 1 Relationship between clinicopathological parameters and TLX1 expression in cancer tissues

Clinicopathological parameters	Low TLX1 expression ($n=15$)	High TLX1 expression ($n=16$)	*p*-value
Age			
< 60	9	8	0.7224
≥ 60	6	8	
Sex			
Male	5	9	0.2852
Female	10	7	
Tumor size (cm)			
< 3	11	5	0.0320*
≥ 3	4	11	
TNM			
I/II	12	5	0.0113*
III/IV	3	11	

Note: TLX1, T-cell leukemia homeobox protein 1; TNM, tumor, node, metastases

efficiency (Supplementary Fig. 1A). CCK-8 assays also confirmed that the knockdown of TLX1 resulted in impaired cell proliferation (Supplementary Fig. 1B), along with a significant reduction in cell migration and invasion (Supplementary Fig. 1C-D).

TLX1 activates TRAPPC9 transcription in HCC

To analyze the downstream mechanisms of TLX1 in HCC, we downloaded the targets of TLX1 from hTFtarget (http://bioinfo.life.hust.edu.cn/hTFtarget/#!/) and intersected with differentially expressed genes in the GSE87410 and GSE105130 datasets on Jvenn (Fig. 3A). Among the eight genes screened out (Fig. 3B), MT2A [15], CRIP1 [16], CCR7 [17], ZFP36 [18], ITGA2 [19], and FAT1 [20] have been reported in HCC, which makes TRAPPC9 and SSR1 as the genes of interests. Since TRAPPC9 (Log_2FoldChange of 1.4729184 in GSE87410 and 0.8031566 in GSE105130) showed a more pronounced high expression, it was chosen as the target of TLX1 in HCC. Subsequent analysis on UCSC (http://genome.ucsc.edu/index.html) revealed a binding peak of TLX1 at the TRAPPC9 promoter (Fig. 3C).

We then examined the TRAPPC9 expression in HCC tissues and their adjacent tissues by RT-qPCR and immunohistochemistry (Fig. 3D, E). The expression of TRAPPC9 was higher in HCC tissues than in matched adjacent tissues. After the patients were divided into two groups with high and low TRAPPC9 expression according to the mean value of TRAPPC9 mRNA expression, we found that the patients with high expression of TRAPPC9 predicted larger tumors and higher tumor staging ($p<0.05$) (Table 2).

Subsequently, RT-qPCR on THLE-, Huh-7 and MHCC97H cells yielded consistent results in vitro (Fig. 3F). We performed ChIP experiments and found enrichment of the TRAPPC9 promoter immunoprecipitated by anti-TLX1, suggesting that TLX1 binds to the promoter of TRAPPC9 (Fig. 3G). Then we predicted the binding site of TLX1 to the TRAPPC9 promoter in the JASPAR database based on the promoter sequence of TRAPPC9 (Fig. 3H). The results of the EMSA assay showed that there was binding between TLX1 and the TRAPPC9 promoter, and the lanes did not show complexes when using the cold probe, whereas the binding between the two disappeared using the probe with the sequence mutation (Fig. 3I), suggesting that TLX1 bound only to the TRAPPC9 promoter. In addition, the luciferase activities of HCC cells transfected with oe-TLX1 were significantly higher than the oe-NC group (Fig. 3J). Finally, RT-qPCR findings revealed that the mRNA expression of TRAPPC9 was restored in HCC cells as well in response to oe-TLX1 infection (Fig. 3K). Finally, we explored whether the knockdown of TLX1 impaired TRAPPC9 transcription and performed knockdown of TRAPPC9 as a positive control. As expected, the knockdown of both TLX1 and TRAPPC9 induced a significant reduction in TRAPPC9 expression (Fig. 3L).

Overexpression of TRAPPC9 abates the repressing effects of TLX1 knockdown on Huh-7 and MHCC97H cell growth.

We further designed experiments to investigate whether TLX1 promotes the malignant behavior of HCC cells in a TRAPPC9-dependent manner. Huh-7 and MHCC97H cells were infected with lentiviruses harboring oe-TRAPPC9 or oe-NC in the presence of sh-TLX1 and verified the overexpression efficacy (Fig. 4A). As the CCK-8 and colony formation assays revealed, overexpression of TRAPPC9 led to enhanced proliferation and colonies formed of Huh-7 and MHCC97H cells (Fig. 4B, C). However, the number of apoptotic cells in the sh-TLX1 + oe-TRAPPC9 group was substantially less than that of sh-TLX1 + oe-NC in the flow cytometric assay, as revealed by the decreased percentage of Annexin V^+PI^- Huh-7 and MHCC97H cells (Fig. 4D). RNF138 has been reported to repress the activation of the NF-κB signaling pathway by preventing the translocation of TRAPPC9 to the cytoplasm in colorectal cancer [21], whereas the NF-κB has been widely associated with proliferation and invasion acceleration and apoptosis inhibition in HCC cells [22]. Therefore, we analyzed NF-κB activation in Huh-7 and MHCC97H cells after overexpression of TLX1 as well as after overexpression of TRAPPC9. The results of western blot analysis showed that after the knockdown of TLX1, the phosphorylation level of P65 was significantly reduced, and the expression of Bcl-2 and Cyclin D1 was significantly decreased. By contrast, after overexpression of TRAPPC9, the P65 phosphorylation as well as Bcl-2 and Cyclin D1 expression were significantly increased (Fig. 4E). In HepG2 and SNU-398 cells, we similarly found that overexpression of TRAPPC9 was

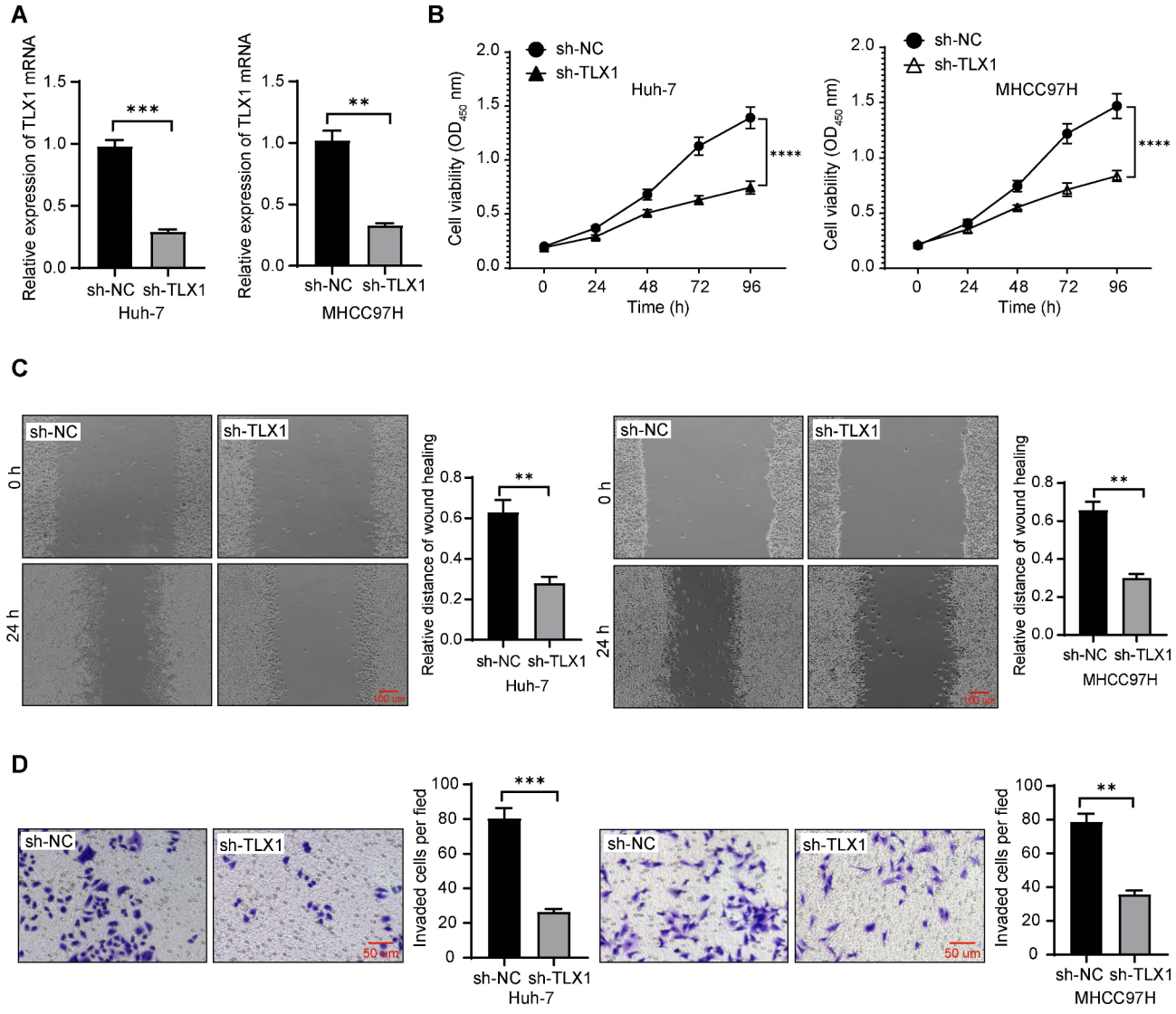

Fig. 2 Knockdown of TLX1 inhibits the biological behavior of Huh-7 and MHCC97H cells. (**A**) The mRNA expression of TLX1 in Huh-7 and MHCC97H cells infected with sh-NC or sh-TLX1 was analyzed using RT-qPCR. (**B**) The OD value of Huh-7 and MHCC97H cells was examined using CCK-8 assays. (**C**) The Huh-7 and MHCC97H cell migration was examined using a wound wound-healing assay. (**D**) The Huh-7 and MHCC97H cell invasion was examined using Transwell assay. Data represent the mean ± SEM of at least three independent experiments. $^{**}p < 0.01$, $^{***}p < 0.001$, $^{****}p < 0.0001$. Differences were tested using an unpaired t-test (**A**, **C**, **D**) and the two-way ANOVA (**B**)

able to reverse the effects of sh-TLX1, with enhanced cell proliferation, increased number of colony formation, and a significantly lower percentage of apoptosis (Supplementary Fig. 2A-D). Likewise, the P65 phosphorylation as well as Bcl-2 and Cyclin D1 expression were significantly increased in HepG2 and SNU-398 cells overexpressing TRAPPC9 as well (Supplementary Fig. 2E).

ZFP69B transcriptionally activates TLX1 expression

We then downloaded TFs with binding sites in the promoter and enhancer regions of TLX1 from GeneCards (https://www.genecards.org/). We compared them with the above two datasets (GSE87410 and GSE105130). Nine intersections were found (Fig. 5A, B) via Jvenn. After excluding EGR2 [23], ZEB2 [24], BCL11B [25], KLF10 [26], EZH2 [27], HIC1 [28], KLF8 [29], ZFP69B (Log2FoldChange: 1.2435806 in GSE87410 and 1.5442059 in GSE105130) was selected as the TF of TLX1 due to its superior expression in the two datasets than ZNF398 (Log2FoldChange: 0.7689866 in GSE87410 and 0.4552225 in GSE105130). ZFP69B was found to have a significant binding peak on the TLX1 promoter region in the UCSC website (Fig. 5C).

As shown by RT-qPCR and immunohistochemistry, the expression of ZFP69B was higher in HCC tissues than in paracarcinoma tissues (Fig. 5D, E). Analysis of the correlation between ZFP69B and clinical information similarly revealed no correlation between ZFP69B and patients'

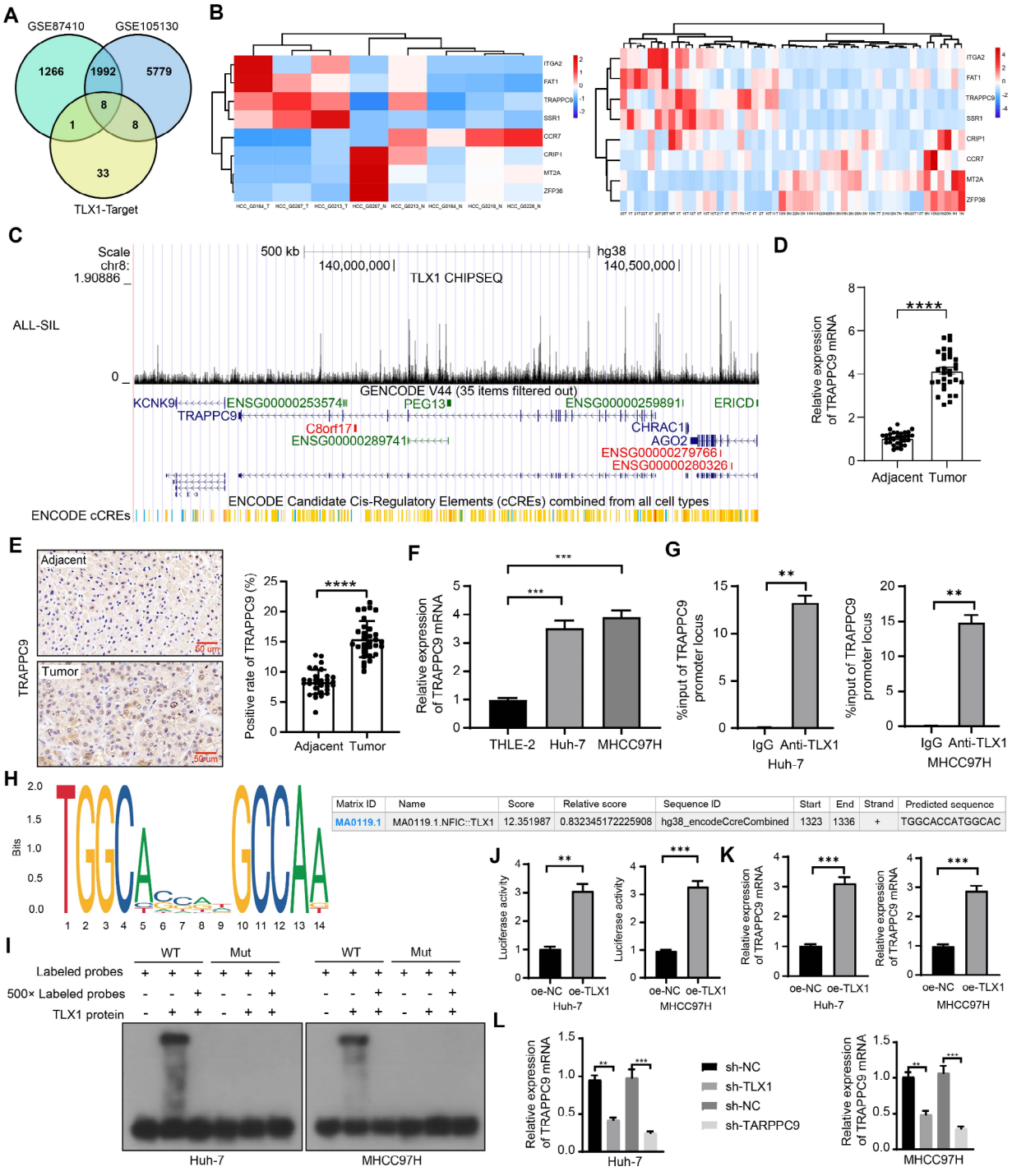

Fig. 3 TLX1 activates TRAPPC9 transcription in HCC cells. (**A**) The intersection of TLX1 downstream targets in hTFtarget and differentially expressed genes in the GSE87410 and GSE105130 datasets. (**B**) The heatmaps of 8 intersecting targets in the three datasets. (**C**) The binding relation between TLX1 and the TRAPPC9 promoter was predicted in the UCSC database. (**D**) Expression of TRAPPC9 mRNA in HCC tissues and their adjacent tissues was analyzed using RT-qPCR ($n = 31$). (E) positive staining of TRAPPC9 in HCC tissues and their adjacent tissues was analyzed using immunohistochemistry ($n = 31$). (**F**) Expression of TRAPPC9 mRNA in THLE-2, Huh-7, and MHCC97H was analyzed using RT-qPCR. (**G**) Enrichment of the TRAPPC9 promoter in HCC cells with anti-TLX1 antibody or anti-IgG control was analyzed using ChIP. (**H**) Jaspar database analysis of binding sites between TLX1 and the TRAPPC9 promoter (**I**) The binding between TLX1 and TRAPPC9 was assessed using EMSA. (**J**) The binding relation between TRAPPC9 and TLX1 was examined using a luciferase reporter assay. (**K**) Expression of TRAPPC9 mRNA in Huh-7 and MHCC97H infected with oe-TLX1 was analyzed using RT-qPCR. (**L**) TRAPPC9 mRNA expression after knockdown of TLX1 or TRAPPC9 in Huh-7 and MHCC97H cells was analyzed using RT-qPCR Data represent the mean ± SEM of at least three independent experiments. $^{**}p < 0.01$, $^{***}p < 0.001$, $^{****}p < 0.0001$. Differences were tested using t-tests (**D**, **E**, **G**, **J**, **K**) and the one-way ANOVA (**F**, **L**)

Table 2 Relationship between clinicopathological parameters and TRAPPC9 expression in cancer tissues

Clinicopathological parameters	Low TRAPPC9 expression ($n=15$)	High TRAPPC9 expression ($n=16$)	p value
Age			
< 60	7	10	0.4795
≥ 60	8	6	
Sex			
Male	8	6	0.4795
Female	7	10	
Tumor size (cm)			
< 3	12	4	0.0038*
≥ 3	3	12	
TNM			
I/II	13	4	0.0010*
III/IV	2	12	

age and sex. By contrast, the mean size of isolated tumors was larger, and the number of patients with stage III/IV was higher in patients with high expression of ZFP69B (Table 3).

Consistently, HCC cells exhibited higher ZFP69B expression than THLE-2 cells (Fig. 5F). ChIP experiments using two HCC cell lines also revealed that ZFP69B bound to the TLX1 promoter (Fig. 5G). Then, we used a luciferase reporter system and found that transfection of the sh-ZFP69B plasmid caused a significant downregulation in luciferase units compared to that in the sh-NC group (Fig. 5H). Similarly, the mRNA expression of TLX1 was reduced in response to sh-ZFP69B (Fig. 5I).

Knockdown of ZFP69B inhibits HCC progression by blocking TLX1/TRAPPC9 signaling

MHCC97H and Huh-7 cells were infected with sh-ZFP69B (sh-NC as control) or sh-ZFP69B+oe-TLX1 (sh-ZFP69B+oe-NC as control). The expression of ZFP69B, TLX1, and TRAPPC9 was examined in HCC cells using RT-qPCR. The expression of three mRNAs was reduced in response to sh-ZFP69B. However, the expression of TLX1 and TRAPPC9 was restored after further overexpression of oe-TLX1, while the ZFP69B remained at the level under sh-ZFP69B treatment alone (Fig. 6A). Knockdown of ZFP69B repressed the HCC cells to grow (Fig. 6B, C), migrate (Fig. 6D), and invade (Fig. 6E). In addition, the apoptosis rate of MHCC97H and Huh-7 cells was enhanced following the knockdown of ZFP69B (Fig. 6F). Meanwhile, overexpression of TLX1 overturned the effects of sh-ZFP69B (Fig. 6B-F).

Huh-7 cells with the above treatments were injected into nude mice to observe tumor growth in vivo. Knockdown of ZFP69B decreased the volume and weight of tumors, while the volume and weight of tumors were upregulated by the concomitant overexpression of TLX1 (Fig. 6G).

Discussion

There is a constant search for improvement in screening, diagnosis, and treatment strategies to improve the prognosis of HCC [30]. In the present study, we found that TLX1 was highly expressed in the HCC tissues and cell lines, and knockdown of TLX1 inhibited the HCC cell viability and mobility. TF ZFP69B induced the expression of TLX1 to promote the transcription of TRAPPC9 in HCC.

The potential function of some genes in the Hox family in the tumor microenvironment and their therapeutic liability in targeted therapy and immunotherapy in HCC have been previously revealed [31], while the role of TLX1 (i.e. HOX11 as we mentioned above) has not been well explained. Akrami et al. found that TLX1 was one of the five genes that can be considered candidate biomarkers or therapeutic targets in pancreatic ductal adenocarcinoma [32]. We also observed the correlation between TLX1 high expression with the larger tumor size and more advanced TNM stage in patients with HCC, indicating its possible biomarker role. Krutikov et al. showed that ectopic TLX1 expression accelerated malignancies in mice deficient in DNA-PK, which was related to dysregulated expression of the cell cycle, apoptotic, and mitotic spindle checkpoint genes [33]. In addition, Bempt et al. revealed that downregulation of TLX1 led to a reduction of target gene expression and induction of leukemia cell death [34]. As Cain et al. summarized, Hox factors ultimately function by manipulating the expression of downstream targets once bound to DNA [35]. Therefore, we sought to identify a target of TLX1 in HCC that might be responsible for its pro-proliferative, pro-migratory, and pro-invasive properties. TRAPPC9 was found to be a candidate with the largest difference in expression in HCC.

TRAPPC9 has been linked to gastric cancer chemoresistance by promoting epithelial-mesenchymal transition [36]. In addition, TRAPPC9 impacts the expression of E-cadherin, CD44, and vimentin via the NF-κB pathways, which makes TRAPPC9 inhibitors possible targets of colorectal cancer in the future [37]. Single nucleotide polymorphism rs11166927 on chromosome 8 in the TRAPPC9 region was reported by Wattacheril et al.to be closely related to the activity score of nonalcoholic fatty liver disease ($p=8.7e-07$) [38] which is emerging as a leading cause of HCC [39]. We, consistently, observed that overexpression of TRAPPC9 induced HCC cell growth and partially prevented the apoptosis in the presence of sh-TLX1.

It has been revealed that six prognosis-related ZNF family genes were independent prognostic factors for the overall survival of patients with esophageal cancer even though ZFP69B was not included [40]. However, it was included in the 12 prognosis-related mRNAs in gastric

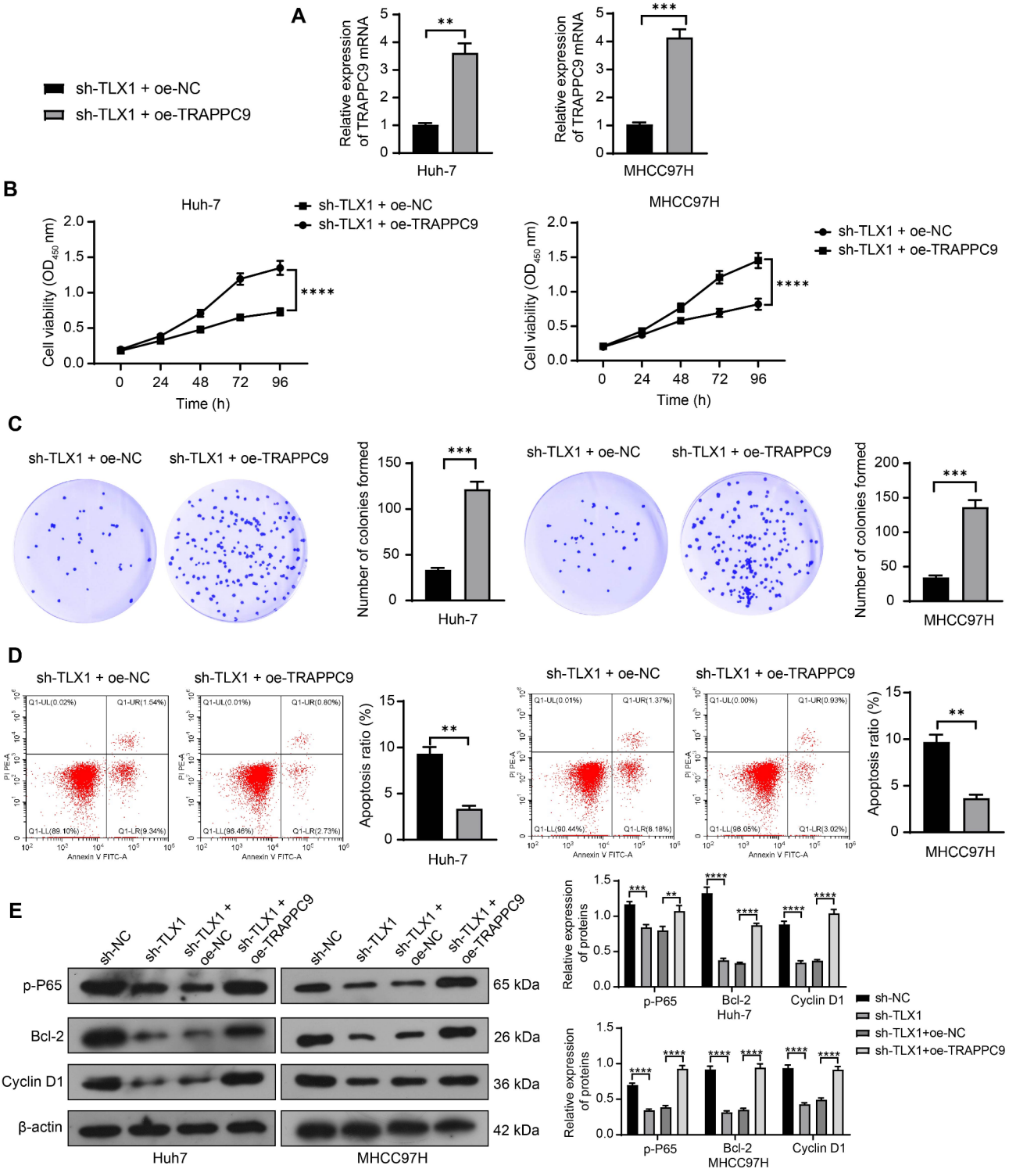

Fig. 4 Overexpression of TRAPPC9 overturns the effects of TLX1 knockdown on Huh-7 and MHCC97H cells. (**A**) Expression of TRAPPC9 mRNA in Huh-7 and MHCC97H in response to sh-TLX1 + oe-NC or sh-TLX1 + oe-TRAPPC9 was analyzed using RT-qPCR. (**B**) The viability of Huh-7 and MHCC97H cells was examined using CCK-8 assays. (**C**) The colony formation of Huh-7 and MHCC97H cells was determined using colony formation assays. (**D**D) The cell apoptosis of Huh-7 and MHCC97H cells was determined using flow cytometry. (**E**) The protein expression of p-P65, Bcl-2, and Cyclin D1 in Huh-7 and MHCC97H cells was determined using western blot analysis. Data represent the mean ± SEM of at least three independent experiments. $^{**}p < 0.01$, $^{***}p < 0.001$, $^{****}p < 0.0001$. Differences were tested using an unpaired t-test (**A**, **C**, **D**) and the two-way ANOVA (**B**, **E**)

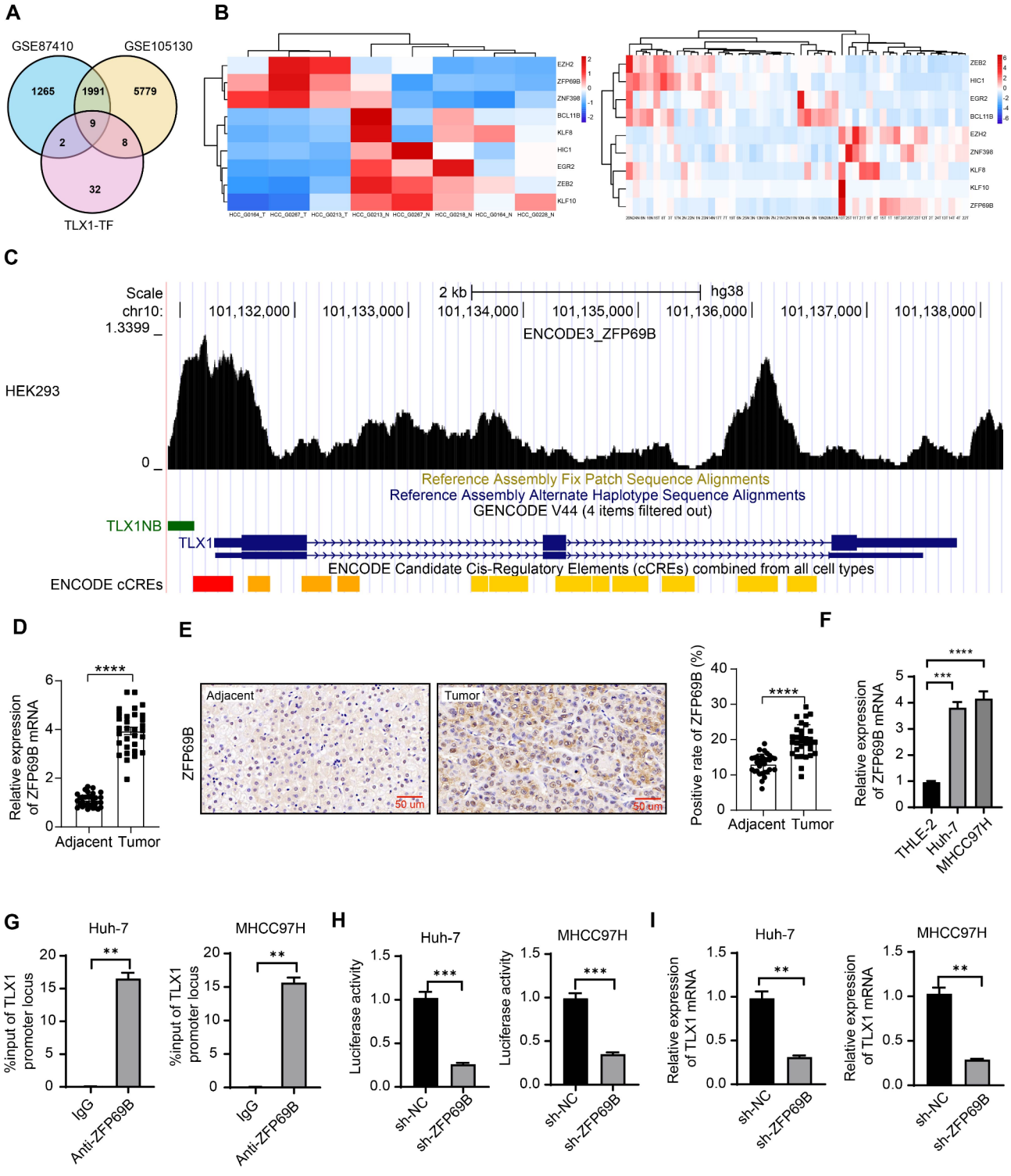

Fig. 5 ZFP69B transcriptionally activates TLX1 expression in HCC cells. (**A**) The intersection of TFs with binding sites in the TLX1 promoter and enhancer regions downloaded on GeneCards and differentially expressed genes in the GSE87410 and GSE105130 datasets. (**B**) The heatmaps of intersecting TF expression in the GSE87410 and GSE105130 datasets. (**C**) The ZFP69B binding peaks on the TLX1 promoter were downloaded from the UCSC database. (**D**) Expression of ZFP69B mRNA in HCC tissues and their adjacent tissues was examined using RT-qPCR ($n = 31$). (**E**) positive staining of ZFP69B in HCC tissues and their adjacent tissues was analyzed using immunohistochemistry ($n = 31$). (**F**) ZFP69B mRNA in THLE-2, Huh-7, and MHCC97H cells was examined using RT-qPCR. (**G**) Enrichment of the TLX1 promoter in HCC cells with anti-ZFP69B antibody or anti-IgG control was analyzed using ChIP. (**H**) The binding relation between ZFP69B and TLX1 was examined using a luciferase reporter assay. (**I**) TLX1 mRNA in Huh-7 and MHCC97H cells infected with sh-ZFP69B was examined using RT-qPCR. Data represent the mean ± SEM of at least three independent experiments. $^{**}p < 0.01$, $^{***}p < 0.001$, $^{****}p < 0.0001$. Differences were tested using a t-test (D, E, G, H, I) and the one-way ANOVA (F)

Table 3 Relationship between clinicopathological parameters and ZFP69B expression in cancer tissues

Clinicopathological parameters	Low ZFP69B expression ($n=14$)	High ZFP69B expression ($n=17$)	*p*-value
Age			
< 60	10	7	0.1493
≥ 60	4	10	
Gender			
Male	6	8	>
Female	8	9	0.9999
Tumor Size (cm)			
< 3	11	5	0.0113*
≥ 3	3	12	
TNM			
I/II	11	6	0.0292*
III/IV	3	11	

cancer [41]. Moreover, ZNF689 expression in HCC and paired-noncancerous tissues was significantly increased compared with that in normal liver tissues, and positive expression of ZNF689 protein in HCC was significantly associated with a tumor size of ≥10 cm, tumor capsule infiltration, and microvascular invasion [42]. We also observed the correlation between ZFP69B and the tumor size and TNM stage of HCC patients ($n=31$). As for the functional role of ZNF members in cancers, ZNF148 was upregulated in breast cancer tissues and cell lines, and the knockdown of ZNF148 suppressed malignant phenotypes, including cell proliferation and tumorigenesis in vitro and in vivo [43]. Oleksiewicz et al. observed that ZFP69B mRNA was associated with diverse immune subtypes and tumor stage, grade, and survival of patients, and ZFP69B positively influenced the cancer cell cycle, migration, and invasion [44]. More relevantly, silencing of ZFP69B reduced proliferation, migration, and invasion, and promoted erastin-induced ferroptosis of HCC cells [45]. However, the in vivo evidence and its molecular targets in HCC are still lacking. Our in vitro and in vivo findings also suggested that the knockdown of ZFP69B led to reduced HCC cell growth, which was reversed by TLX1 overexpression.

In the future, other downstream targets of TLX1 besides TRAPPC9, for instance, Notch1 [46] are required to be identified to corroborate the function of TLX1 in HCC. In addition, orthotopic xenograft mouse models which can better reflect the HCC tumorigenesis [47, 48] might further support our conclusion from subcutaneous implantation.

In conclusion, we showed a previously unrecognized role of ZFP69B in the regulation of TRAPPC9 via the TF TLX1 and induced HCC development. Furthermore, this study provides a molecular basis and rationale for targeting the ZFP69B/TLX1/TRAPPC9 axis as a novel therapeutic strategy to treat HCC.

Materials and methods

Data acquisition and preprocessing

Transcriptomic differences in 3 HCC tumor tissues and 5 normal tissues (platform no. GPL11154) in the GSE87410 dataset and paired 25 tumors and adjacent 27 non-tumors (platform no. GPL11154) in the GSE105130 dataset were analyzed with the GEO2R for analysis. The *p-value* was corrected using Benjamini & Hochberg (False discovery rate), and the threshold was set to adj. *p*. value < 0.05. We downloaded the list of human TF and human TF cofactors from the HumanTFDB (http://bioinfo.life.hust.edu.cn/HumanTFDB#!/download) database. KEGG pathway enrichment analysis was performed with the aid of the Hiplot (https://hiplot.com.cn/) tool, again using Benjamini & Hochberg for *p*-value correction, setting the pathway enrichment threshold at adj. *p*. value < 0.05. UCSC (http://genome.ucsc.edu/index.html) was used to analyze ChIP-seq data to explore the enrichment of TLX1 at the TRAPPC9 promoter or ZFP69B at the TLX1 promoter. The Jaspar database (https://jaspar.genereg.net/) was used to analyze the binding sites between TLX1 and the TRAPPC9 promoter.

Patients and specimens

The study was approved by the Medical Ethics Committee of Jurong Hospital Affiliated to Jiangsu University, and all patients were informed. We collected 31 paired HCC and matched adjacent (3 cm) non-tumor liver tissues from patients who underwent surgical treatment from September 2018 to December 2023 at Jurong Hospital Affiliated to Jiangsu University. All patients were diagnosed according to the 2018 Practice Guidance by the American Association for the Study of Liver Diseases [49]. Inclusion criteria were as follows: (i) patients were ≥18 years old and ≤70 years old or had the full civil capacity to provide informed consent; (ii) no history of preoperative anticancer radiotherapy or chemotherapy, biological, immunological, or herbal treatments; (iii) complete postoperative follow-up data; and (iv) no history of malignant tumors or systemic immune diseases in other organs.

Immunohistochemistry

Collected HCC tissues and non-tumor liver tissues were heated in sodium citrate buffer for antigen retrieval and incubated with 3% hydrogen peroxide for 30 min to remove endogenous peroxidase before being sealed with 5% goat serum for 1 h. The sections were incubated with antibodies against TLX1 (1:50, ab191270, Abcam, Cambridge, UK), TRAPPC9 (1:100, PA5-106442, Thermo Fisher Scientific Inc., Waltham, MA, USA), ZFP69B (1:500, PA5-60667, Thermo Fisher Scientific) overnight at 4 °C. The sections were then incubated with the secondary antibody goat anti-rabbit IgG (1:100, GTX213110-01,

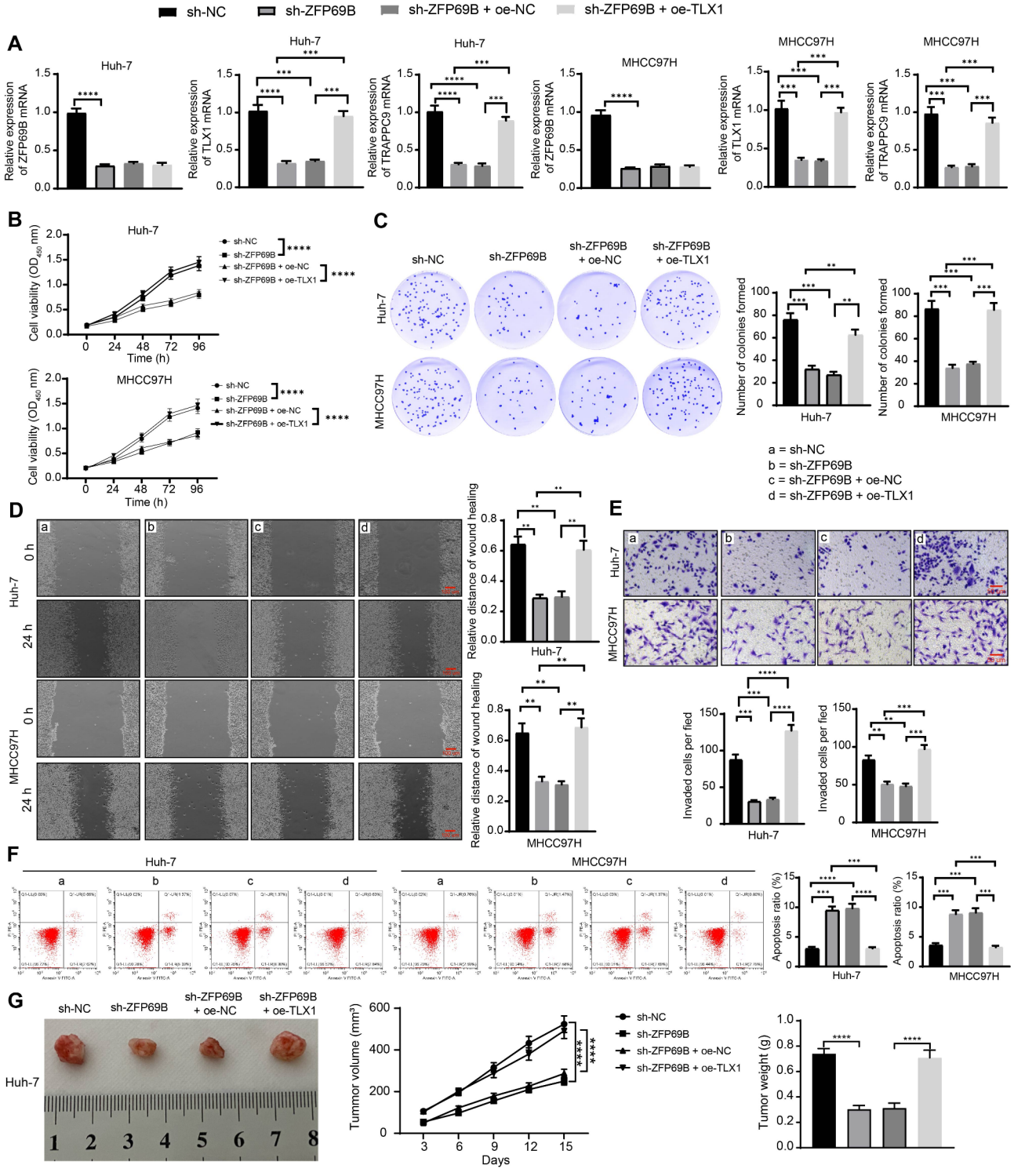

Fig. 6 Knockdown of ZFP69B inhibits HCC progression by blocking the TLX1/TRAPPC9 signaling. (**A**) The mRNA expression of ZFP69B, TLX1, and TRAPPC9 in HCC cells infected with sh-NC, sh-ZFP69B, sh-ZFP69B + oe-NC or sh-ZFP69B + oe-TLX1 was examined using RT-qPCR. (**B**) The viability of HCC cells was examined using CCK-8 assays. (**C**) The colony formation of HCC cells was determined using colony formation assays. (**D**) The migration of HCC cells was examined using a wound wound-healing assay. (**E**) The invasion of HCC cells was examined using Transwell invasion assays. (**F**) The cell apoptosis of HCC cells was determined using flow cytometry. (**G**) The volume and weight of xenografts of tumor-bearing mice. Data represent the mean ± SEM of at least three independent experiments or five biological replicates. $^{**}p < 0.01$, $^{***}p < 0.001$, $^{****}p < 0.0001$. Differences were tested using the one-way (**A**, **C**, **D**, **E**, **F**) or two-way ANOVA (**B**, **G**)

GeneTex, Inc., Alton Pkwy Irvine, CA, USA), and the positively-stained area in the tissues was observed via microscopy after DAB staining and hematoxylin staining.

Cell culture and infection

MHCC97H (C6585) and HepG2 (C6346) purchased from Beyotime Biotechnology Co., Ltd. (Shanghai, China), and Huh-7 (BNCC337690) purchased from BeNa Culture Collection (Beijing, China) were cultured in DMEM with 10% fetal bovine serum (FBS) added (BNCC338068, BeNa). SNU-398 (SNL-517) cells were purchased from Sunncell (Wuhan, Hubei, China) and grown in RPMI-1640 medium (SNLM-517, Sunncell) supplemented with 10% FBS. Transformed human liver epithelial-2 (THLE-2) cells (CL-0833) were purchased from Procell (Wuhan, Hubei, China) and cultured in a specialized medium (CM-0833) provided by the manufacturer. The culture environment was maintained at 37 °C with 5% CO_2.

The lentiviral vectors containing sh-ZFP69B (ACCAA AGAGTCAGCCTTACAGAATGATATTTCGTGGGA AGA), sh-TLX1 (AGAGGCGTCCCGCACCTGTCTG AACTGTTAAGAAATCTGTT), sh-TRAPPC9 (CAGC GACTTCCCTTTGGCCATAGAAAGAAATGGTGA GCATG), overexpression (oe)-TLX1, and oe-TRAPPC9 were purchased from Thermo Fisher Scientific. Huh7, MHCC97H, HepG2, and SNU-398 cells were infected with lentiviruses containing sh-ZFP69B, sh-TLX1, oe-TLX1, oe-TRAPPC9, negative control (sh-NC), and no specific cDNA (oe-NC), respectively, for 24 h. Alternatively, the Huh7 and MHCC97H cells were infected with sh-NC, sh-TLX1, or sh-TRAPPC9 for 24 h. Puromycin (2.5 μg/mL, A1113803, Thermo Fisher Scientific) was then used to screen for stable cells.

Cell viability assay

Cell counting kit-8 (CCK-8) (C0037, Beyotime) was used to examine Huh-7, MHCC97H, HepG2, and SNU-398 cell proliferation. The cells were plated at 2×10^3 per well and incubated with CCK-8 reagent. The optical density (OD) at 450 nm at 24 h, 48 h, 72 h, and 96 h was read using a microplate reader.

Wound healing assay

The Huh-7, MHCC97H, HepG2, and SNU-398 cells were cultured until the formation of a confluent monolayer, and the serum-free culture medium was added to inhibit cell proliferation. Next, using a pipette, a clean scratch wound was created across the center of each well. The medium was aspirated, and the cells were washed 3 more times with sterile PBS to wash away the scratched cells. The plates were incubated in an incubator at 37 °C for 24 h, allowing for the migration of cells. Changes in wound width were recorded by light microscopy.

Transwell invasion assay

Huh-7, MHCC97H, HepG2, and SNU-398 cells (1×10^5 cells/well) were starved overnight, and then serum-free culture medium was added to the apical chamber chambers in 96-well Transwell plates (pore size 8 μm, CLS3374-2EA, Merck Millipore, Darmstadt, Germany) coated with Matrigel (356234, Beijing Solarbio Life Sciences Co., Ltd., Beijing, China). The basolateral chamber was filled with DMEM. The cells were incubated at 37℃ for 48 h, fixed with 10% glutaraldehyde at 4℃ for 30 min, stained with 1% crystal violet for 20 min at room temperature, and visualized under a microscope.

Flow cytometry analysis

The number of apoptotic cells in Huh-7, MHCC97H, HepG2, and SNU-398 cells was detected by flow cytometry using the Annexin V-FITC Apoptosis Detection Kit (Merck). The cells were stained with Annexin V-FITC and PI in the dark. After washing, they were analyzed using flow cytometry and Flowjo software.

Colony formation assay

Each group of cells (300 cells/well) was cultured in 6-well plates at 37 °C for 2 weeks. The formed cell colonies were fixed with 4% formaldehyde for 15 min at room temperature, stained with 1% crystal violet for 20 min at room temperature, and counted.

Chromatin immunoprecipitation (ChIP) assay

The ChIP kit was purchased from Thermo Fisher Scientific (26156). MHCC97H and Huh-7 cells were treated with 1% formaldehyde for 10 min at room temperature. Glycine at 0.125 M was added and maintained for 5 min to terminate the cross-linking. Chromatin in the lysate was cleaved into fragments with an average length of 300–500 bp using ultrasound, and anti-ZFP69B (Cusabio, Wuhan, Hubei, China), anti-TLX1 (1:1, sc-12760X, Santa Cruz Biotechnology Inc., Santa Cruz, CA, USA), or IgG (ab172730, Abcam) were used to immunoprecipitate the samples overnight at 4 °C. The DNA fragments obtained by immunoprecipitation were purified. Then, qPCR was performed to detect the degree of enrichment of promoter fragments therein.

Dual-luciferase reporter assay

Genomic fragments containing TLX1 and TRAPPC9 promoter regions were amplified into pGL4.20 (Promega Corporation, Madison, WI, USA) basic vector, respectively. A reporter gene vector containing the TLX1 promoter was transfected into Huh-7 and MHCC97H cells with sh-NC or sh-ZFP69B. A reporter gene vector containing the TRAPPC9 promoter was transfected into Huh-7 and MHCC97H cells with oe-TLX1 or oe-NC.

After 24 h of transfection, luciferase activity was detected using a luciferase assay kit (RG005, Beyotime).

Electrophoresis mobility shift assay (EMSA)

To confirm the binding relationship between TLX1 and the TRAPPC9 promoter, we designed 5' biotin-tagged oligonucleotides of the TLX1 promoter and customized recombinant proteins of TLX1 at Thermo Fisher. EMSA was then performed using the LightShift Chemiluminescent EMSA Kit (20148, Thermo Fisher) according to the instructions. Briefly, biotin-labeled oligonucleotides were incubated with TLX1 recombinant protein in binding buffer (1× binding buffer, 2.5% glycerol, 5 mmol/L MgCl2, 50 ng/μL Poly(dI: dC), and 0.05% NP-40) for 20 min at room temperature. The resulting protein-DNA complexes were electrophoresed and transferred to a nylon membrane. Biotin-labeled DNA was detected using streptavidin/horseradish peroxidase conjugate. To confirm the specificity of TLX1 binding to the TRAPPC9 promoter, we used a 500-fold excess of cold probe as a control.

In vivo tumor model

The experimental protocol was approved by the Ethics Committee for Animal Experiments of Jurong Hospital Affiliated to Jiangsu University. BALB/C nude mice (6-week-old, male) were purchased from Vital River (Beijing, China). Briefly, 2.0×10^6 Huh-7 cells suspended in 50 μL PBS were subcutaneously injected into the mice. Tumor volumes of mice were examined 3, 6, 9, 12, and 15 days after injection, and mice in each group were euthanized after 15 days by an overdose of pentobarbital (125 mg/kg). The weight and size of the tumors were determined to indicate the tumorigenic capacity of Huh-7 cells with different treatments. The tumor volume was calculated using the formula: Volume = length × width^2/2.

RT-quantitative PCR analysis

Total RNA was extracted from THLE-2, Huh-7, MHCC97H, HepG2, and SNU-398 cells using TRIzol reagent (15596026, Thermo Fisher Scientific), and cDNA synthesis was performed using the RevertAid RT kit (K1691; Thermo Fisher Scientific). RT-qPCR was performed using Fast SYBR (4385610, Thermo Fisher Scientific) to quantify the ZFP69B, TLX1, and TRAPPC9 transcript levels. Data were analyzed using the $2^{-\Delta\Delta CT}$ calculation method. The primer sequences were as follows: ZFP69B forward, 5'-GGAGAAGAACCATGGCTG ATGG-3' and reverse 5'-GCCACAATGTAGTTCTTCC CACG-3'; TLX1 forward, 5'- GGTCAAAACCTGGTTC CAGAACC-3' and reverse 5'- TGTGCCAGGCTCTTCT GGAAGG-3'; TRAPPC9 forward, 5'-TGGCATCAACCC TGACACCAGT-3' and reverse 5'-AGGACACGTACAG CCTTGATGC-3'; GAPDH forward, 5'-GTCTCCTCTG ACTTCAACAGCG-3' and reverse 5'-ACCACCCTGTT GCTGTAGCCAA-3'.

Western blot and antibodies

Treated HCC cells were lysed with lysis buffer (15 mmol/L Tris-HCl pH = 7.5, 150 mmol/L NaCl, 0.1% Tween 20, and 1 mmol/L DTT) supplemented with protease inhibitors for 25 min on ice and centrifuged to collect total proteins. The protein concentration was quantified using a BCA protein assay kit. Proteins were separated via SDS-polyacrylamide gel electrophoresis. Next, samples were transferred to polyvinylidene difluoride (PVDF) membranes. Non-specific binding sites on the membranes were blocked for 1 h with 5% non-fat milk. After blocking, membranes were incubated first with primary antibodies to p-P65 (1:1000, ab76302, Abcam), Bcl2 (1:2000, ab182858, Abcam), Cyclin D1 (1:20, MA5-16356, Thermo Fisher Scientific) and β-actin (1:5000, GTX110564, GeneTex) and then with horseradish peroxidase-coupled goat anti-rabbit IgG antibody (1:100, GTX213110-01, GeneTex) for 2 h at room temperature. Finally, immunoreactions were visualized using an ECL substrate.

Statistics

Data are shown as mean ± standard error of the mean unless otherwise indicated. GraphPad Prism 8.0.2 (GraphPad, San Diego, CA, USA) software was used for statistical analysis. Fisher's exact test was used to analyze the correlation between two categorical variables. Paired or unpaired t-tests and ANOVA, followed by Tukey's or Sidak's multiple comparison tests, were performed for 2 groups and 3 groups, respectively. $p<0.05$ was considered significant.

Abbreviations

HCC	Hepatocellular carcinoma
TLX1	T-cell leukemia homeobox protein 1
ZFP69B	Zinc finger protein 69 homolog B
TRAPPC9	Trafficking protein particle complex subunit 9
DMEM	Dulbecco's modified eagle's medium
CCK-8	Cell counting kit-8
OD	Optical density
ChIP	Chromatin immunoprecipitation

Supplementary Information

The online version contains supplementary material available at https://doi.org/10.1186/s13008-024-00131-z.

Supplementary Material 1

Supplementary Material 2

Author contributions

WX and ZMB designed the study and drafted the manuscript. DY and YY were primarily responsible for collecting data, performing data analysis, and revising

the manuscript. WX, ZMB, DY, and YY performed the experiments. All authors read and approved the final manuscript.

Funding
Financial support was provided by the Guiding Project for Social Development in Zhenjiang City (Number FZ2019019).

Data availability
The datasets used or analyzed are available from the corresponding author upon reasonable request.

Declarations

Ethics approval and consent to participate
The study was approved by the Medical Ethics Committee of Jurong Hospital Affiliated to Jiangsu University, and all patients were informed. The experimental protocol was approved by the Ethics Committee for Animal Experiments of Jurong Hospital Affiliated to Jiangsu University.

Consent for publication
Not applicable.

Competing interests
The authors declare no competing interests.

Received: 16 May 2024 / Accepted: 29 August 2024
Published online: 11 September 2024

References

1. Sung H, Ferlay J, Siegel RL, et al. Global Cancer statistics 2020: GLOBOCAN estimates of incidence and Mortality Worldwide for 36 cancers in 185 countries. CA Cancer J Clin. 2021;71(3):209–49.
2. Ito T, Nguyen MH. Perspectives on the underlying etiology of HCC and its effects on Treatment outcomes. J Hepatocell Carcinoma. 2023;10:413–28.
3. Vogel A, Meyer T, Sapisochin G, Salem R, Saborowski A. Hepatocellular carcinoma. Lancet. 2022;400(10360):1345–62.
4. Chakraborty E, Sarkar D. Emerging therapies for Hepatocellular Carcinoma (HCC). Cancers (Basel). 2022; 14(11).
5. Brown ZJ, Tsilimigras DI, Ruff SM, et al. Management of Hepatocellular Carcinoma: a review. JAMA Surg. 2023;158(4):410–20.
6. Wanninger A. Hox, homology, and parsimony: an organismal perspective. Semin Cell Dev Biol. 2024;152–153:16–23.
7. Feng Y, Zhang T, Wang Y, et al. Homeobox genes in cancers: from carcinogenesis to recent therapeutic intervention. Front Oncol. 2021;11:770428.
8. Bardelli V, Arniani S, Pierini V et al. T-Cell Acute Lymphoblastic Leukemia: biomarkers and their clinical usefulness. Genes (Basel). 2021; 12(8).
9. Wang X, He H, Rui W, Xie X, Wang D, Zhu Y. Long non-coding RNA BCAR4 binds to miR-644a and targets TLX1 to promote the progression of bladder Cancer. Onco Targets Ther. 2020;13:2483–90.
10. Mbimba T, Hussein NJ, Najeed A, Safadi FF. TRAPPC9: novel insights into its trafficking and signaling pathways in health and disease (review). Int J Mol Med. 2018;42(6):2991–7.
11. Sui C, Song Z, Yu H, Wang H. Prognostic significance of TPX2 and NIBP in esophageal cancer. Oncol Lett. 2019;18(4):4221–9.
12. Li X, Han M, Zhang H, et al. Structures and biological functions of zinc finger proteins and their roles in hepatocellular carcinoma. Biomark Res. 2022;10(1):2.
13. He L, Fan X, Li Y, et al. Overexpression of zinc finger protein 384 (ZNF 384), a poor prognostic predictor, promotes cell growth by upregulating the expression of cyclin D1 in hepatocellular carcinoma. Cell Death Dis. 2019;10(6):444.
14. Zhao C, Zhang Z, Jing T. A novel signature of combing cuproptosis- with ferroptosis-related genes for prediction of prognosis, immunologic therapy responses and drug sensitivity in hepatocellular carcinoma. Front Oncol. 2022;12:1000993.
15. Li H, Lu YF, Chen H, Liu J. Dysregulation of metallothionein and circadian genes in human hepatocellular carcinoma. Chronobiol Int. 2017;34(2):192–202.
16. Wang J, Zhou Y, Zhang D, et al. CRIP1 suppresses BBOX1-mediated carnitine metabolism to promote stemness in hepatocellular carcinoma. EMBO J. 2022;41(15):e110218.
17. Yang L, Chang Y, Cao P. CCR7 preservation via histone deacetylase inhibition promotes epithelial-mesenchymal transition of hepatocellular carcinoma cells. Exp Cell Res. 2018;371(1):231–7.
18. Krohler T, Kessler SM, Hosseini K et al. The mRNA-binding Protein TTP/ZFP36 in Hepatocarcinogenesis and Hepatocellular Carcinoma. Cancers (Basel). 2019; 11(11).
19. Wang L, Gao Y, Zhao X, et al. HOXD3 was negatively regulated by YY1 recruiting HDAC1 to suppress progression of hepatocellular carcinoma cells via ITGA2 pathway. Cell Prolif. 2020;53(8):e12835.
20. Huang ZL, Zhang PB, Zhang JT, Li F, Li TT, Huang XY. Comprehensive genomic profiling identifies FAT1 as a negative Regulator of EMT, CTCs, and Metastasis of Hepatocellular Carcinoma. J Hepatocell Carcinoma. 2023;10:369–82.
21. Lu Y, Huang R, Ying J, et al. RING finger 138 deregulation distorts NF-small ka, CyrillicB signaling and facilities colitis switch to aggressive malignancy. Signal Transduct Target Ther. 2022;7(1):185.
22. Gupta R, Kadhim MM, Turki Jalil A, et al. Multifaceted role of NF-kappaB in hepatocellular carcinoma therapy: molecular landscape, therapeutic compounds and nanomaterial approaches. Environ Res. 2023;228:115767.
23. Liu Z, Pu Y, Bao Y, He S. Investigation of potential molecular biomarkers for diagnosis and prognosis of AFP-Negative HCC. Int J Gen Med. 2021;14:4369–80.
24. Zhang L, Xu J, Zhou S, et al. Endothelial DGKG promotes tumor angiogenesis and immune evasion in hepatocellular carcinoma. J Hepatol. 2024;80(1):82–98.
25. Abe H, Kamimura K, Okuda S, et al. BCL11B expression in hepatocellular carcinoma relates to chemosensitivity and clinical prognosis. Cancer Med. 2023;12(14):15650–63.
26. Yoo SH, Nahm JH, Lee WK, Lee HW, Chang HY, Lee JI. Loss of Kruppel-like factor-10 facilitates the development of chemical-induced liver cancer in mice. Mol Med. 2023;29(1):156.
27. Wang B, Liu Y, Liao Z, Wu H, Zhang B, Zhang L. EZH2 in hepatocellular carcinoma: progression, immunity, and potential targeting therapies. Exp Hematol Oncol. 2023;12(1):52.
28. Ceccarelli V, Ronchetti S, Marchetti MC, et al. Molecular mechanisms underlying eicosapentaenoic acid inhibition of HDAC1 and DNMT expression and activity in carcinoma cells. Biochim Biophys Acta Gene Regul Mech. 2020;1863(2):194481.
29. Wang MD, Xing H, Li C, et al. A novel role of Kruppel-like factor 8 as an apoptosis repressor in hepatocellular carcinoma. Cancer Cell Int. 2020;20:422.
30. Pinero F, Dirchwolf M, Pessoa MG. Biomarkers in Hepatocellular Carcinoma: diagnosis, Prognosis and Treatment Response Assessment. Cells 2020; 9(6).
31. Yi C, Wei W, Wan M, Chen Y, Zhang B, Wu W. Expression patterns of HOX Gene Family defines Tumor Microenvironment and Immunotherapy in Hepatocellular Carcinoma. Appl Biochem Biotechnol. 2023;195(8):5072–93.
32. Akrami S, Tahmasebi A, Moghadam A, Ramezani A, Niazi A. Integration of mRNA and protein expression data for the identification of potential biomarkers associated with pancreatic ductal adenocarcinoma. Comput Biol Med. 2023;157:106529.
33. Krutikov K, Zheng Y, Chesney A, et al. Ectopic TLX1 expression accelerates malignancies in mice deficient in DNA-PK. PLoS ONE. 2014;9(2):e89649.
34. Vanden Bempt M, Demeyer S, Broux M et al. Cooperative enhancer activation by TLX1 and STAT5 drives development of NUP214-ABL1/TLX1-Positive T cell Acute Lymphoblastic Leukemia. Cancer Cell. 2018; 34(2); 271 – 85 e7.
35. Cain B, Gebelein B. Mechanisms underlying hox-mediated transcriptional outcomes. Front Cell Dev Biol. 2021;9:787339.
36. Fu ZH, Liu SQ, Qin MB, et al. NIK– and IKKbeta–binding protein contributes to gastric cancer chemoresistance by promoting epithelial–mesenchymal transition through the NF–kappaB signaling pathway. Oncol Rep. 2018;39(6):2721–30.
37. Xu CY, Qin MB, Tan L, Liu SQ, Huang JA. NIBP impacts on the expression of E-cadherin, CD44 and vimentin in colon cancer via the NF-kappaB pathway. Mol Med Rep. 2016;13(6):5379–85.
38. Wattacheril J, Lavine JE, Chalasani NP et al. Genome-Wide Associations Related to Hepatic Histology in Nonalcoholic Fatty Liver Disease in Hispanic Boys. J Pediatr. 2017; 190; 100-7 e2.
39. Polyzos SA, Chrysavgis L, Vachliotis ID, Chartampilas E, Cholongitas E. Nonalcoholic fatty liver disease and hepatocellular carcinoma: insights in epidemiology, pathogenesis, imaging, prevention and therapy. Semin Cancer Biol. 2023;93:20–35.

40. Hong K, Yang Q, Yin H, Wei N, Wang W, Yu B. Comprehensive analysis of ZNF family genes in prognosis, immunity, and treatment of esophageal cancer. BMC Cancer. 2023;23(1):301.
41. Zheng X, Wang X, Zheng L, et al. Construction and analysis of the Tumor-Specific mRNA-miRNA-lncRNA network in gastric Cancer. Front Pharmacol. 2020;11:1112.
42. Yi PS, Wu B, Deng DW, Zhang GN, Li JS. Positive expression of ZNF689 indicates poor prognosis of hepatocellular carcinoma. Oncol Lett. 2018;16(4):5122–30.
43. Wang Y, Gong Y, Li X, et al. Targeting the ZNF-148/miR-335/SOD2 signaling cascade triggers oxidative stress-mediated pyroptosis and suppresses breast cancer progression. Cancer Med. 2023;12(23):21308–20.
44. Oleksiewicz U, Machnik M, Sobocinska J et al. ZNF643/ZFP69B exerts Oncogenic Properties and Associates with Cell Adhesion and Immune processes. Int J Mol Sci. 2023; 24(22).
45. Wang Q, Wang B, Ma X, et al. Identification of a Novel ferroptosis-related gene signature for Predicting Prognosis and responsiveness to Immunotherapy in Hepatocellular Carcinoma. J Hepatocell Carcinoma. 2023;10:1–16.
46. Hounjet J, Van Aerschot L, De Keersmaecker K, Vooijs M, Kampen KR. The DMT1 isoform lacking the iron-response element regulates normal and malignant hematopoiesis via NOTCH pathway activation. FEBS Lett. 2024;598(12):1506–12.
47. Huang M, Long J, Yao Z, et al. METTL1-Mediated m7G tRNA modification promotes Lenvatinib Resistance in Hepatocellular Carcinoma. Cancer Res. 2023;83(1):89–102.
48. Tang H, Dilimulati D, Yang Z, et al. Chemically engineered mTOR-nanoparticle blockers enhance antitumour efficacy. EBioMedicine. 2024;103:105099.
49. Marrero JA, Kulik LM, Sirlin CB, et al. Diagnosis, staging, and management of Hepatocellular Carcinoma: 2018 Practice Guidance by the American Association for the study of Liver diseases. Hepatology. 2018;68(2):723–50.

Publisher's note